

Enantioselective Topological Frequency Conversion

Kai Schwennicke and Joel Yuen-Zhou

*Department of Chemistry and Biochemistry, University of California,
San Diego, La Jolla, California 92093, United States*

Two molecules are enantiomers if they are non-superimposable mirror images of each other. Electric dipole-allowed cyclic transitions $|1\rangle \rightarrow |2\rangle \rightarrow |3\rangle \rightarrow |1\rangle$ obey the symmetry relation $\mathcal{O}^R = -\mathcal{O}^S$, where $\mathcal{O} = (\boldsymbol{\mu}_{21} \cdot \mathbf{E}_{21})(\boldsymbol{\mu}_{13} \cdot \mathbf{E}_{13})(\boldsymbol{\mu}_{32} \cdot \mathbf{E}_{32})$, and R, S label the two enantiomers. Here we generalize the concept of topological frequency conversion to an isotropic ensemble of molecular enantiomers. We show that, within a rotating-frame, the pumping power between fields of frequency ω_1 and ω_2 is sensitive to enantiomeric excess, $\mathcal{P}_{2 \rightarrow 1} = \hbar \frac{\omega_1 \omega_2 \langle C_-^R \rangle}{2\pi} (N_R - N_S)$, where N_i is the number of enantiomers i and $\langle C_-^R \rangle \propto \text{sgn} \mathcal{O}^R$ is an isotropically averaged Chern number. Connections with chiroptical microwave spectroscopy are made.

Introduction.— In the mid nineteenth century, Louis Pasteur discovered that molecules can possess handedness, or chirality, an attribute that influences how they interact with their surroundings [1]. The two species of a chiral molecule, referred to as enantiomers, are nonsuperimposable mirror images of each other and, while they feature many identical physicochemical properties (up to very small parity violation corrections [2]), they can also exhibit drastically different behavior when exposed to chiral environments or stimuli. Thus, enantioselectivity plays a crucial role in biological activity as well as in the synthesis, purification, and characterization of pharmaceuticals [3–5]. Traditionally, optical rotation and circular dichroism have served as optical tools to obtain enantioselective information; however, these techniques rely on the weak interaction between molecules and the magnetic component of the optical field. To bypass these limitations, techniques that rely solely on electric dipole interactions [6] have been recently advocated. For instance, many efforts are currently invested in photoelectron circular dichroism [7–9]. Yet, others focus on nonlinear optical signals that depend on the sign of the electric fields with which the molecules interact [10, 11] including photoexcitation circular dichroism [12], the use of synthetic chiral fields [13–16], and microwave three-wave mixing [17–21]. More precisely, the latter technique can be understood through cyclic three-level models [22–28] where the product of three light-matter couplings [hereafter referred to as the Kral-Shapiro (KS) product] differs by a π phase between the two enantiomers. This remarkable symmetry has been exploited to propose cyclic population transfer schemes [22, 28] or the use of cross-polarized terahertz pulses [29] to prepare the enantiomers in different energy configurations or orientations for separation. This symmetry has also been utilized to suggest an enantioselective generalization of the Stern-Gerlach [30] or spin Hall [31] experiments, where spatial separation of enantiomers,

rather than spins, is achieved using artificial gauge fields [32–34]. The analogy between enantiomer and spin labels is intriguing and surprisingly underexplored, and serves as the motivation of our present work. More specifically, we wish to demonstrate an enantioselective analogue to the Quantum Spin Hall Effect (QSHE) [35].

On the other hand, since the pioneering work of Thouless, Kohmoto, Nightingale, and den Nijs in relation to the Quantum Hall Effect (QHE) [36], notions of symmetry-protected topological phases (SPTPs) have been at the heart of condensed matter research, and have only been exacerbated in the past fifteen years with the discovery of topological insulators [37]. These notions guarantee that certain response properties of so-called topologically non-trivial systems are largely independent of material specification, instead depending only on products of universal constants and integer quantities known as topological invariants. The discrete nature of these properties implies that they are robust against material imperfections, thus making them attractive for metrology, among other applications. While topological protection was originally identified in translationally invariant 2D systems, its scope has been enlarged through the use of Floquet engineering in systems of different dimensionality [38–41]. Of particular interest is a elegant construction due to Martin, Refael, and Halperin [42], where quantized "current" is observed. In this Letter, we design a novel spectroscopic scheme that generalizes TFC to the microwave spectroscopy of an isotropic ensemble of chiral molecules. The resulting signal is proportional to enantiomeric excess (EE), with a simple prefactor containing the sign of the KS product, thus providing, as far as we are aware, the first link between the fields of chiroptical spectroscopy and topological phases of matter. Owing to the topological nature of the signal, it should also serve as a very sensitive detection of EE.

Model.— Consider a chiral molecule hosting a three-

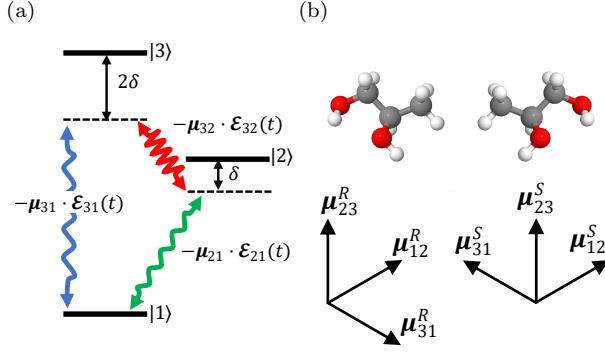


Figure 1: *The model.* (a) Cyclic three-level transitions in molecules that lack inversion symmetry, such as enantiomers. Three near-resonant lasers with modulated field amplitudes $\mathcal{E}_{ij}(t)$ interact with these transitions. (b) Transition-dipole moments for the R - and S -1,2-propanediol enantiomers. Note that the three dipoles are mutually orthogonal.

level system as shown in Fig. 1. The ground state $|1\rangle$ and the two excited states $|2\rangle$, $|3\rangle$, with energies $\hbar\epsilon_1$, $\hbar\epsilon_2$, $\hbar\epsilon_3$, are coupled to each other using a set of three orthogonally-polarized time-dependent electric fields

$$\begin{aligned}\mathbb{E}_{21}(t) &= \mathcal{E}_{21}(t) \cos(\Omega_{21}t), \\ \mathbb{E}_{32}(t) &= \mathcal{E}_{32}(t) \cos(\Omega_{32}t), \\ \mathbb{E}_{31}(t) &= \mathcal{E}_{31}(t) \sin(\Omega_{31}t),\end{aligned}\quad (1)$$

where the frequencies $\Omega_{21} = \epsilon_2 - \epsilon_1 - \delta$, $\Omega_{32} = \epsilon_3 - \epsilon_2 - \delta$, $\Omega_{31} = \epsilon_3 - \epsilon_1 - 2\delta$, are slightly detuned from the system's natural frequencies, and the field amplitudes $\mathcal{E}_{21}(t)$, $\mathcal{E}_{32}(t)$, $\mathcal{E}_{31}(t)$ are slowly modulated. As we shall see, it is crucial that the three fields are polarized along three mutually orthogonal directions, so that the non-linear optical signal survives orientational averaging [43]. Assuming that $|\boldsymbol{\mu}_{ij} \cdot \mathcal{E}_{ij}(t)|/2 \ll \hbar\Omega_{ij}$, the Hamiltonian for this laser-dressed system, after making the rotating wave approximation, is

$$H(t) = \sum_{i=1}^3 \hbar\epsilon_i - \sum_{i>j} \boldsymbol{\mu}_{ij} \cdot \mathcal{E}_{ij}(t) \left(\frac{e^{-i(\Omega_{ij}t + \phi_{ij})}}{2} |i\rangle\langle j| + \text{h.c.} \right), \quad (2)$$

where $\boldsymbol{\mu}_{ij}$ is the transition-dipole moment for $|j\rangle \rightarrow |i\rangle$, and $\phi_{21} = \phi_{32} = 0$ and $\phi_{31} = \frac{\pi}{2}$. The associated time-dependent wavefunction of the system is $|\psi(t)\rangle$.

Next, we consider the rotating frame

$$U(t) = e^{-i(\epsilon_2 - \Omega_{21})t} |1\rangle\langle 1| + e^{-i\epsilon_2 t} |2\rangle\langle 2| + e^{-i(\epsilon_2 + \Omega_{32})t} |3\rangle\langle 3|, \quad (3)$$

such that $|\psi(t)\rangle = U(t)|\tilde{\psi}(t)\rangle$. In this frame, $i\hbar|\dot{\tilde{\psi}}(t)\rangle = \mathcal{H}(t)|\tilde{\psi}(t)\rangle$, with the effective Hamiltonian:

$$\mathcal{H}(t) = \frac{1}{2} \begin{pmatrix} -2\hbar\delta & -\boldsymbol{\mu}_{21} \cdot \mathcal{E}_{21}(t) & i\boldsymbol{\mu}_{31} \cdot \mathcal{E}_{31}(t) \\ -\boldsymbol{\mu}_{21} \cdot \mathcal{E}_{21}(t) & 0 & -\boldsymbol{\mu}_{32} \cdot \mathcal{E}_{32}(t) \\ -i\boldsymbol{\mu}_{31} \cdot \mathcal{E}_{31}(t) & -\boldsymbol{\mu}_{32} \cdot \mathcal{E}_{32}(t) & 2\hbar\delta \end{pmatrix} \quad (4)$$

. This analysis is similar to Ref. [44] where the In the complex basis $|+\Pi\rangle, |0\rangle, |-\Pi\rangle$, where $|\pm\Pi\rangle = \frac{1}{\sqrt{2}}(|1\rangle \pm i|3\rangle)$ and $|0\rangle = |2\rangle$, Eq. 4 becomes

$$\begin{aligned}\mathcal{H}(t) &= -\frac{\boldsymbol{\mu}_{21} \cdot \mathcal{E}_{21}(t)}{2} L_x - \frac{\boldsymbol{\mu}_{32} \cdot \mathcal{E}_{32}(t)}{2} L_y \\ &\quad - \frac{\boldsymbol{\mu}_{31} \cdot \mathcal{E}_{31}(t)}{2} L_z - \frac{\delta}{2\hbar} (L_+^2 + L_-^2)\end{aligned}\quad (5)$$

where $L_x = \frac{1}{\sqrt{2}} \begin{pmatrix} 0 & 1 & 0 \\ 1 & 0 & 1 \\ 0 & 1 & 0 \end{pmatrix}$, $L_y = \frac{1}{\sqrt{2}} \begin{pmatrix} 0 & -i & 0 \\ i & 0 & -i \\ 0 & i & 0 \end{pmatrix}$,

$L_z = \begin{pmatrix} 1 & 0 & 0 \\ 0 & 0 & 0 \\ 0 & 0 & -1 \end{pmatrix}$ are the angular momentum opera-

tors for a spin-1 particle and $L_+ = \begin{pmatrix} 0 & \hbar\sqrt{2} & 0 \\ 0 & 0 & \hbar\sqrt{2} \\ 0 & 0 & 0 \end{pmatrix}$,

$L_- = \begin{pmatrix} 0 & 0 & 0 \\ \hbar\sqrt{2} & 0 & 0 \\ 0 & \hbar\sqrt{2} & 0 \end{pmatrix}$ are the corresponding ladder

operators. Hereafter, we will assume that the slowly-modulated electric field amplitudes are

$$\begin{aligned}\mathcal{E}_{21}(t) &= \mathbf{E}_{21} \sin(\omega_1 t), \\ \mathcal{E}_{32}(t) &= \mathbf{E}_{32} \sin(\omega_2 t), \\ \mathcal{E}_{31}(t) &= \mathbf{E}_{31} [m - \cos(\omega_1 t) - \cos(\omega_2 t)],\end{aligned}\quad (6)$$

where m is a scalar. These functional forms are inspired from the TFC scheme reported in [44].

TFC. — For completeness, we briefly rederive the TFC formalism using adiabatic perturbation theory (the original paper does so within Floquet theory [42]). In the rotating frame, the rate of the system's energy absorption is given by $\dot{E} = \langle \tilde{\psi}(t) | \dot{\mathcal{H}}(t) | \tilde{\psi}(t) \rangle$. In the long time limit, $t \rightarrow \infty$, the time-averaged energy-absorption rate, or average power, is

$$\mathcal{P}_{av} = \lim_{t \rightarrow \infty} \frac{1}{t} \int_0^t dt \dot{E} = \sum_{\omega_i} \mathcal{P}_{av}(\omega_i), \quad (7a)$$

$$\mathcal{P}_{av}(\omega_i) = \lim_{t \rightarrow \infty} \frac{1}{t} \int_0^t dt' \omega_i \langle \partial_{\omega_i t'} \mathcal{H}(t') \rangle, \quad (7b)$$

where $\mathcal{P}_{av}(\omega_i)$ is the average power at the modulation frequency ω_i .

Let $|\epsilon_l(t)\rangle$ denote the l -th adiabatic state of $\mathcal{H}(t)$, where $\mathcal{H}(t)|\epsilon_l(t)\rangle = \epsilon_l(t)|\epsilon_l(t)\rangle$ (Fig. 2). The total wavefunction in the rotating frame can be written as $|\tilde{\psi}(t)\rangle = \sum_l \tilde{c}_l(t) |\epsilon_l(t)\rangle$. Near the adiabatic

limit where ω_1, ω_2 are much smaller than the instantaneous energy gap of $\mathcal{H}(t)$, and if the system is initiated in the l -th adiabatic state, *i.e.*, $|\tilde{\psi}(0)\rangle = |\epsilon_l(0)\rangle$, the total wavefunction to first order in the modulation frequencies is

$$|\tilde{\psi}(t)\rangle = e^{-i\phi_l(t)} \left[|\epsilon_l(t)\rangle - i\hbar \sum_{l' \neq l} \frac{|\epsilon_{l'}(t)\rangle \langle \epsilon_{l'}(t) | \boldsymbol{\omega} \cdot \nabla_{\boldsymbol{\omega}} | \epsilon_l(t) \rangle}{\epsilon_l(t) - \epsilon_{l'}(t)} \right], \quad (8a)$$

$$\phi_l(t) = \frac{1}{\hbar} \int_{t_0}^t dt' \epsilon_l(t') - i\hbar \langle \epsilon_l(t) | \boldsymbol{\omega} \cdot \nabla_{\boldsymbol{\omega}} | \epsilon_l(t) \rangle, \quad (8b)$$

where $\boldsymbol{\omega} = (\omega_1, \omega_2)$. If ω_1, ω_2 are incommensurate, *i.e.*, ω_1/ω_2 is irrational, $\mathcal{H}(t)$ is not periodic. However, if we write $\mathcal{H}(t) = \mathcal{H}(\boldsymbol{\theta}) = \mathcal{H}(\theta_1, \theta_2)$ with $\theta_i = \omega_i t \pmod{2\pi}$, we notice that $\mathcal{H}(\boldsymbol{\theta})$ is quasiperiodic, $\mathcal{H}(\theta_1 + 2\pi, \theta_2) = \mathcal{H}(\theta_1, \theta_2 + 2\pi) = \mathcal{H}(\theta_1, \theta_2)$, and the domain of $\mathcal{H}(\theta_1, \theta_2)$ is a two-dimensional torus $\mathbb{T} = [0, 2\pi) \otimes [0, 2\pi)$. To first order in $\boldsymbol{\omega}$, the expected quantities $\langle \partial_{\omega_1 t} \mathcal{H}(t) \rangle$ and $\langle \partial_{\omega_2 t} \mathcal{H}(t) \rangle$ for $|\tilde{\psi}(t)\rangle$ given in Eq. 8a are

$$\langle \partial_{\omega_1 t} \mathcal{H}(t) \rangle = \langle \partial_{\theta_1} \mathcal{H}(\boldsymbol{\theta}) \rangle = \partial_{\theta_1} \epsilon_l(\boldsymbol{\theta}) - \hbar \omega_2 \Omega_l(\boldsymbol{\theta}) \quad (9a)$$

$$\langle \partial_{\omega_2 t} \mathcal{H}(t) \rangle = \langle \partial_{\theta_2} \mathcal{H}(\boldsymbol{\theta}) \rangle = \partial_{\theta_2} \epsilon_l(\boldsymbol{\theta}) + \hbar \omega_1 \Omega_l(\boldsymbol{\theta}) \quad (9b)$$

where $\Omega_l(\boldsymbol{\theta}) = i \langle \partial_{\theta_1} \epsilon_l(\boldsymbol{\theta}) | \partial_{\theta_2} \epsilon_l(\boldsymbol{\theta}) \rangle + \text{h.c.}$ is the Berry curvature of the l -th adiabatic band (see Supplemental Material Section I, SM-I [45]).

According to the mean-value theorem for incommensurate ω_1, ω_2 [48], the linear flow of $\boldsymbol{\theta}$ covers the torus densely for long enough times. Thus, the time average of the function $F(t)$ is the same as the average of $F(\boldsymbol{\theta})$ over the entire torus \mathbb{T} :

$$\lim_{t \rightarrow \infty} \frac{1}{t} \int_0^t dt F(t) = \frac{1}{4\pi^2} \int_{\mathbb{T}} d\boldsymbol{\theta} F(\boldsymbol{\theta}). \quad (10)$$

Substituting Eqs. 9a-9b into Eq. 7b gives rise to the average power lost by the fields at ω_1, ω_2 when the system is initiated in the l -th band, $\mathcal{P}_{av}(\omega_1) = -\mathcal{P}_{av}(\omega_2) = -\frac{\hbar \omega_1 \omega_2 C_l}{2\pi}$. Here the average of $\partial_{\theta_i} \epsilon_l(\boldsymbol{\theta})$ is zero since $\epsilon_l(\boldsymbol{\theta})$ is quasiperiodic in $\boldsymbol{\theta}$, and $C_l = \frac{1}{2\pi} \int_{\mathbb{T}} d\boldsymbol{\theta} \Omega_l(\boldsymbol{\theta})$ is the Chern number of the l -th band. Thus, the average energy-pumping rate between the two modulation fields $\mathcal{P}_{2 \rightarrow 1} = [\mathcal{P}_{av}(\omega_2) - \mathcal{P}_{av}(\omega_1)]/2$ is quantized,

$$\mathcal{P}_{2 \rightarrow 1} = \frac{\hbar \omega_1 \omega_2 C_l}{2\pi}, \quad (11)$$

or in other words, after one period of the ω_2 modulation, C_l photons with frequency ω_1 are produced. The very off-resonant nature of this process guarantees that the molecule does not retain energy and

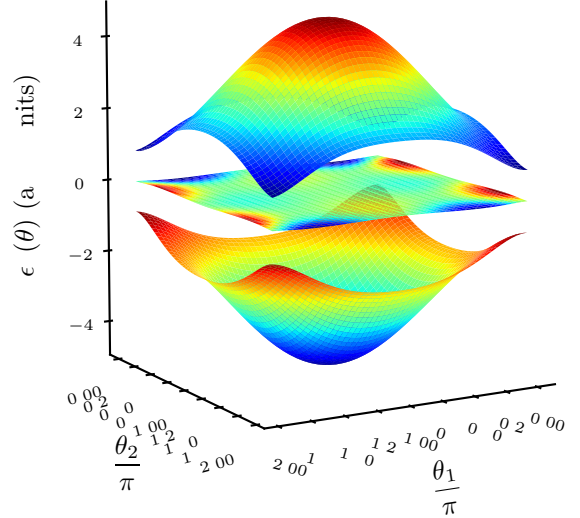


Figure 2: Example adiabatic bands giving rise to enantioselective TFC. The color gradient is a visual aid.

the energy transfer process occurs only between the fields.

Enantioselective TFC. — For $\delta = 0$, $\mathcal{H}(\boldsymbol{\theta})$ (see Eq. 5), resembles half of the Bernevig-Hughes-Zhang Hamiltonian [49], except that the Pauli matrices are replaced with the spin-1 angular momentum operators. As expected, $\mathcal{H}(\boldsymbol{\theta})$ is topologically non-trivial for $|m| < 2$, where the Chern numbers for the lower (L) and upper (U) adiabatic bands remarkably acquire the value,

$$C_L = 2 \text{sgn}(m) \text{sgn}(\mathcal{O}) = -C_U, \quad (12)$$

and that for the middle (M) band is $C_M = 0$ (for an analytical proof, see SM-II [45]). $\mathcal{O} = (\boldsymbol{\mu}_{21} \cdot \mathbf{E}_{21})(\boldsymbol{\mu}_{13} \cdot \mathbf{E}_{13})(\boldsymbol{\mu}_{32} \cdot \mathbf{E}_{32})$ is the KS product which obeys the enantioselective symmetry relation $\mathcal{O}^R = -\mathcal{O}^S$, and we have assumed $\mathbf{E}_{ij} = \mathbf{E}_{ji}$. The aforementioned symmetry holds for systems with broken inversion symmetry, which chiral molecules fulfill. Therefore $C_L^R = -C_L^S$, and the TFC for the two enantiomers initiated in the lower (upper) adiabatic band at $t = 0$ is expected to have the same magnitude but opposite sign, *i.e.*, $\mathcal{P}_{2 \rightarrow 1}^R = -\mathcal{P}_{2 \rightarrow 1}^S$. This results begs us to consider the fruitful analogy between enantiomer label and spin degrees of freedom. Just like in the QSHE, where the transverse conductivity for opposite spins bears opposite signs, so does the TFC for opposite enantiomers. Eq. 12 is the central result of this letter and relates a fundamental topological invariant from chiroptical spec-

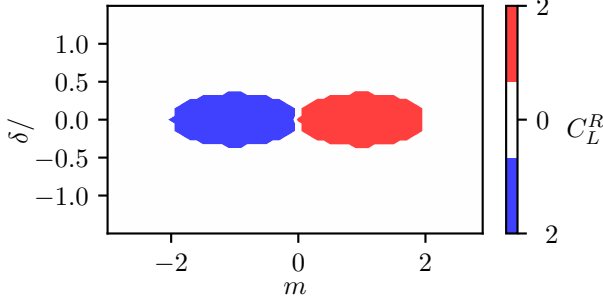


Figure 3: *Topological phase diagram.* The value of C_L^R is calculated taking the magnitudes of the light-matter couplings to be equal, *i.e.*

$|\boldsymbol{\mu}_{21} \cdot \mathbf{E}_{21}| = |\boldsymbol{\mu}_{32} \cdot \mathbf{E}_{32}| = |\boldsymbol{\mu}_{31} \cdot \mathbf{E}_{31}| = \hbar D$, while the laser-driving parameters m and δ are varied. We obtain $C_L^R = 2\text{sgn}(m)\text{sgn}(\mathcal{O}^R)$ at the vicinity of $\delta = 0$, where $\mathcal{O}^R = -\mathcal{O}^S$ is the Kral-Shapiro product, which is enantioselective.

troscopy ($\text{sgn}\mathcal{O} = \pm 1$) with the notions of SPTPs. Fig. 3 shows the computed value of C_L^R for different values of m when $\delta \neq 0$.

By analogy with Eq. 7, we can compute the average power absorbed in the original frame (Eq. 3) as $P_{av}(\Omega) = \lim_{t \rightarrow \infty} \frac{1}{t} \int_0^t dt' \Omega \langle \partial_{\Omega t'} H(t') \rangle$, obtaining:

$$\frac{P_{av}(\omega_1)}{\hbar\omega_1} = \frac{P_{av}(\Omega_{21+1})}{\hbar\Omega_{21+1}} - \frac{P_{av}(\Omega_{21-1})}{\hbar\Omega_{21-1}} + \frac{P_{av}(\Omega_{31+1})}{\hbar\Omega_{31+1}} - \frac{P_{av}(\Omega_{31-1})}{\hbar\Omega_{31-1}}, \quad (13a)$$

$$\frac{P_{av}(\omega_2)}{\hbar\omega_1} = \frac{P_{av}(\Omega_{32+2})}{\hbar\Omega_{32+2}} - \frac{P_{av}(\Omega_{32-2})}{\hbar\Omega_{32-2}} + \frac{P_{av}(\Omega_{31+2})}{\hbar\Omega_{31+2}} - \frac{P_{av}(\Omega_{31-2})}{\hbar\Omega_{31-2}}, \quad (13b)$$

where $\Omega_{ij\pm 1,2} = \Omega_{ij} \pm \omega_{1,2}$. Thus, the quantization due to the enantioselective TFC can be extracted from an experimentally detected difference power spectrum of the fields interacting with the molecule. Notice that the topology is preserved for $\delta \neq 0$ as long as $\hbar|\delta| < |\boldsymbol{\mu}_{ij} \cdot \mathbf{E}_q|/2$.

Numerical results. — The dynamics of the system is calculated by numerically integrating the Schrödinger equation in the rotating frame (Eq. 4), and the power spectrum is obtained by returning to the original frame. In atomic units ($\hbar = 1$), the electric field amplitudes are taken to be $\mathbf{E}_{21} = 5E_0\hat{x}$, $\mathbf{E}_{32} = 3E_0\hat{y}$, $\mathbf{E}_{31} = E_0\hat{z}$, where $E_0 = 4.0 \times 10^{-9}$ a.u., the transition-dipole moments are $\boldsymbol{\mu}_{21}^R = \boldsymbol{\mu}_{21}^S = 0.75$ a.u. \hat{x} , $\boldsymbol{\mu}_{32}^R = \boldsymbol{\mu}_{32}^S = 0.47$ a.u. \hat{y} , $\boldsymbol{\mu}_{31}^R = -\boldsymbol{\mu}_{31}^S = 0.14$ a.u. \hat{z} , and the molecular transition energies are $\epsilon_2 - \epsilon_1 = 4.4 \times 10^{-8}$ a.u. and $\epsilon_3 - \epsilon_1 = 4.7 \times 10^{-8}$ a.u. The transition-dipole moments and molecular energies are extracted from a microwave three-wave-mixing model for R - and

S -1,2-propanediol [17]. Using these parameters, it is true that $|\boldsymbol{\mu}_{ij} \cdot \mathbf{E}_{ij}|/2 \ll \hbar\Omega_{ij}$, so the rotating wave approximation holds. The slow incommensurate modulation frequencies and laser detuning are taken to be $\omega_1 = \omega_2/\phi = \delta = 1 \times 10^{-11}$ a.u., where we take $\phi = \frac{\sqrt{5}-1}{2}$, satisfying the perturbative condition $\hbar\delta, \hbar\omega_1, \hbar\omega_2 \ll |\boldsymbol{\mu}_{ij} \cdot \mathbf{E}_{ij}|/2$. Setting $m = 1.4$, the system is in the topologically nontrivial regime.

To obtain the desired enantioselective TFC, both enantiomers need to be prepared in the lowest adiabatic bands in the rotating frame at $t = 0$. Suppose that before fields are turned on ($\boldsymbol{\mu}_{ij} \cdot \mathbf{E}_{ij}(t) \rightarrow 0$ as $t \rightarrow -\infty$), the molecules start at $|1\rangle$. Under those circumstances, the eigenstates of Eq. 4 are the states $|1\rangle, |2\rangle, |3\rangle$ with eigenenergies $\epsilon_{L,M,U}(-\infty) = -\delta, 0, \delta$, and the state of each molecule is $|\epsilon_L(-\infty)\rangle$. If the electric fields are slowly turned on at a rate ω_r that is much smaller than the instantaneous band gaps $|\epsilon_l(t) - \epsilon_{l'}(t)|$, both enantiomers are prepared in $|\epsilon_L(0)\rangle$. Note that the modulating frequencies ω_1, ω_2 must also be much smaller than $|\epsilon_l(t) - \epsilon_{l'}(t)|$ at all times. Chirped laser fields for $t < 0$ satisfy this constraint. The adiabatic protocol we choose is $\mathbf{E}_{ij} \rightarrow \mathbf{E}_{ij}\alpha(t)$ and $\omega_{1,2} \rightarrow \omega_{1,2}\beta(t)$, where the ramp-up functions slowly vary at the rate $\omega_r = 2 \times 10^{-13}$ a.u.

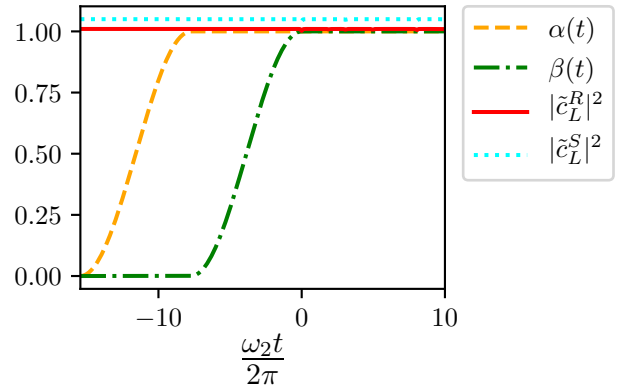


Figure 4: *Adiabatic state preparation.* Presented are the plots for the functions $\alpha(t)$ and $\beta(t)$. We also feature the populations $|\tilde{c}_L^R|^2$, $|\tilde{c}_L^S|^2$ (shifted vertically slightly to be visible) of the lower adiabatic state for each enantiomer. As shown, the system is effectively prepared in the lower adiabatic bands for both enantiomers.

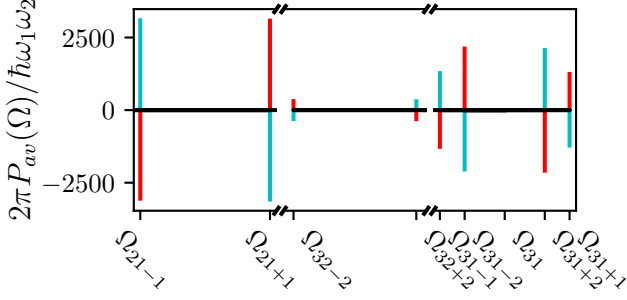


Figure 5: *Enantioselective TFC*. Plotted is the difference power spectrum for the driving electric field when coupled to the R - (red) and S - (cyan) 1,2-propanediol enantiomers. This spectrum is enantioselective, and the TFC rate is topological, $\frac{2\pi}{\hbar\omega_1\omega_2}\mathcal{P}_{2\rightarrow 1}^R = -\frac{2\pi}{\hbar\omega_1\omega_2}\mathcal{P}_{1\rightarrow 2}^S = 2$.

(see Fig. 4),

$$\alpha(t) = \begin{cases} 0 & t < -\frac{2\pi}{\omega_r}, \\ \frac{1-\cos\omega_r t}{2} & -\frac{2\pi}{\omega_r} < t < -\frac{\pi}{\omega_r}, \\ 1 & -\frac{\pi}{\omega_r} < t, \end{cases} \quad (14a)$$

$$\beta(t) = \begin{cases} 0 & t < -\frac{\pi}{\omega_r}, \\ \frac{1+\cos\omega_r t}{2} & -\frac{\pi}{\omega_r} < t < 0, \\ 1 & 0 < t. \end{cases} \quad (14b)$$

After a sufficiently long time (we choose $t^* = 2000 \times 2\pi/\omega_2$), the frequency-resolved time-averaged power spectrum $P_{av}(\Omega)$ lost by the fields is numerically calculated considering only $t \geq 0$. This quantity is indeed enantioselective, and using Eqs. 13a and 13b, each enantiomer Chern number for the lower band $C_L^R = 2 = -C_L^S$ is extracted, revealing the topological nature of this nonlinear optical phenomenon (Fig. 5).

Oriental averaging. — Since we are interested in an isotropic ensemble of molecules, the orientationally averaged Chern number for the R - enantiomer is numerically calculated,

$$\langle C_L^R \rangle = \frac{1}{8\pi^2} \int_0^{2\pi} \int_0^{2\pi} \int_0^\pi d\chi d\phi d\theta C_-^R(\chi, \phi, \theta) \sin(\theta), \quad (15)$$

where the molecule's orientation with respect to the driving electric field is specified by the Euler angles χ, ϕ, θ . After performing Monte Carlo integration simulations, a 95% confidence interval is used to calculate the expectation value and error for the distribution of orientationally averaged Chern numbers (see SM-III [45]). It is found that $\langle C_L^R \rangle = 1.311 \pm 0.001$, suggesting that even for an isotropic ensemble of molecules, the enantioselective TFC survives (interestingly, for $\delta \rightarrow 0$, we obtain the simple

result $\langle C_L^R \rangle = 1.333 \pm 0.001$, which we conjecture to be $\langle C_L^R \rangle = \frac{4}{3}$, although we cannot analytically prove it). Then, the expected pumping rate for an isotropic ensemble containing N_R R -molecules and N_S S -molecules is

$$\mathcal{P}_{2\rightarrow 1} = \frac{\hbar\omega_1\omega_2 \langle C_L^R \rangle}{2\pi} (N_R - N_S). \quad (16)$$

which is zero for a racemic mixture, but otherwise, reveals the EE $N_R - N_S$. Notice that in line with other nonlinear chiroptical signals that depend on electric but not magnetic dipole contributions [6], Eq. (16) contains no background achiral signal, unlike traditional circular dichroism, where both enantiomers have the same electric dipole and magnetic dipole absorption strengths for circularly polarized light [50].

Let us briefly discuss potential sources of noise in the proposed enantioselective TFC. First, the linewidths of microwave transitions are on the order of 10-100 kHz [51], which are smaller than the adiabatic state preparation gap $\delta \approx 1$ MHz, as well as the light-matter interactions $|\boldsymbol{\mu}_{ij} \cdot \mathbf{E}_{ij}|/\hbar \approx 10$ MHz inducing the topological gap, or even the smallest difference in energies in the power spectrum (see, Fig. 5, $\Omega_{31\pm 1} - \Omega_{31\pm 2} \approx 1$ MHz). Thus, the described protocol should be resilient to the finite linewidths of these transitions. Another source of imperfections stems from laser shot noise. Assuming that the laser beam waist area is ~ 1 cm² and considering the field strength above, the shot noise for a time interval t^* is $\sim 10^9$ (see SM-IV [45]). From the power spectrum (Fig. 5), we find that for the same time interval, that the minimal magnitude of the change in the photon number due to the TFC is $\min\left(\left|\frac{P_{av}(\Omega_{ij\pm 1,2})t^*}{\hbar\Omega_{ij\pm 1,2}}\right|\right) \approx 100 \times |N_R - N_S|$. Therefore, as long as the magnitude of the enantiomer excess $|N_R - N_S|$ is much larger than $\sim 10^7$, the signal should be detectable above the shot noise. These arguments indicate that an experimental observation of enantioselective TFC should be realizable and could be used for chiral discrimination.

Conclusion. — In summary, we have presented an enantioselective TFC setup for an ensemble of chiral molecules. Owing to the dependence of the topological invariant on the sign of the KS product (Eq. 12), which differs by a phase of π for the two enantiomers, the quantized time-averaged energy-pumping rate is of opposite sign for the R - and S - molecules, just like transverse conductivity is of opposite sign for up and down spins in the QSHE. We show that the computed signal survives orientational averaging for any sample with EE and vanishes for a racemic mixture. An intriguing consequence of Eq. 11 is that as long as the timescale separations required by the model are fulfilled, the chemical identity of

the probed molecules (*e.g.*, through the strengths of the transition dipole moments) in the rotating frame is erased by the signal, leading to a universal nonlinear optical response which acknowledges the enantiomeric excess only. This characteristic is reminiscent to the very accurate determination of the quantum of conductance with a wide range of QHE systems. Thus, from a metrological standpoint, the generality of the enantioselective TFC can be exploited to accurately measure EE by running a linear fit of the pumping rate $\mathcal{P}_{2 \rightarrow 1}$ for a series of experiments where ω_1 (or ω_2) is varied. Furthermore, if one is only concerned with $|\text{EE}|$, there is no need to calibrate the signal with an enantiopure sample beforehand.

While concepts of topology have been very productive in the exploration of new condensed matter physics phenomena, most of them are restricted to periodic solids (see Ref. [52, 53] for a few molec-

ular exceptions). TFC [40, 42] is a powerful tool that opens doors to the application of those concepts to 0D systems such as finite molecular systems. In particular, this work reveals that laser-dressed chiral molecules support SPTs that are not adiabatically connected to their non-laser-dressed counterparts.

ACKNOWLEDGMENTS

K.S. and J.Y.-Z. were supported by NSF CAREER CHE 1654732. This work employed computational resources of the Extreme Science and Engineering Discovery Environment (XSEDE), which is supported by National Science Foundation Grant No. ACI-1548562, under allocation No. TG-ASC150024. K.S. acknowledges helpful discussions with Matthew Du, Stephan van den Wildenberg, and Jorge A. Campos-González-Angulo.

-
- [1] L. Pasteur, *Annales Chimie Phys.* **24**, 442 (1848).
 - [2] M. Quack, J. Stohner, and M. Willeke, *Annu. Rev. Phys. Chem.* **59**, 741 (2008).
 - [3] A. Hutt and S. Tan, *Drugs* **52**, 1 (1996).
 - [4] B. Kasprzyk-Hordern, *Chemical Society Reviews* **39**, 4466 (2010).
 - [5] D. G. Blackmond, *Cold Spring Harbor perspectives in biology* **2**, a002147 (2010).
 - [6] A. F. Ordonez and O. Smirnova, *Physical Review A* **98**, 063428 (2018).
 - [7] I. Powis, *The Journal of Chemical Physics* **112**, 301 (2000).
 - [8] N. Böwering, T. Lischke, B. Schmidtke, N. Müller, T. Khalil, and U. Heinzmann, *Physical review letters* **86**, 1187 (2001).
 - [9] P. V. Demekhin, A. N. Artemyev, A. Kastner, and T. Baumert, *Physical review letters* **121**, 253201 (2018).
 - [10] P. Fischer, D. S. Wiersma, R. Righini, B. Champagne, and A. D. Buckingham, *Physical review letters* **85**, 4253 (2000).
 - [11] P. Brumer, E. Frishman, and M. Shapiro, *Physical Review A* **65**, 015401 (2001).
 - [12] S. Beaulieu, A. Comby, D. Descamps, B. Fabre, G. Garcia, R. Généaux, A. Harvey, F. Légaré, Z. Mašín, L. Nahon, *et al.*, *Nature Physics* **14**, 484 (2018).
 - [13] O. Neufeld, D. Ayuso, P. Decleva, M. Y. Ivanov, O. Smirnova, and O. Cohen, *Physical Review X* **9**, 031002 (2019).
 - [14] D. Ayuso, O. Neufeld, A. F. Ordonez, P. Decleva, G. Lerner, O. Cohen, M. Ivanov, and O. Smirnova, *Nature Photonics* **13**, 866 (2019).
 - [15] O. Neufeld, M. E. Tzur, and O. Cohen, *Physical Review A* **101**, 053831 (2020).
 - [16] D. Ayuso, A. Ordonez, P. Decleva, M. Ivanov, and O. Smirnova, *arXiv preprint arXiv:2004.05191* (2020).
 - [17] D. Patterson, M. Schnell, and J. M. Doyle, *Nature* **497**, 475 (2013).
 - [18] D. Patterson and J. M. Doyle, *Physical review letters* **111**, 023008 (2013).
 - [19] V. A. Shubert, D. Schmitz, D. Patterson, J. M. Doyle, and M. Schnell, *Angewandte Chemie International Edition* **53**, 1152 (2014).
 - [20] S. Lobsiger, C. Perez, L. Evangelisti, K. K. Lehmann, and B. H. Pate, *The journal of physical chemistry letters* **6**, 196 (2015).
 - [21] V. A. Shubert, D. Schmitz, C. Pérez, C. Medcraft, A. Krin, S. R. Domingos, D. Patterson, and M. Schnell, *The journal of physical chemistry letters* **7**, 341 (2016).
 - [22] P. Král and M. Shapiro, *Physical Review Letters* **87**, 183002 (2001).
 - [23] P. Král, I. Thanopoulos, M. Shapiro, and D. Cohen, *Physical review letters* **90**, 033001 (2003).
 - [24] I. Thanopoulos, P. Král, and M. Shapiro, *The Journal of chemical physics* **119**, 5105 (2003).
 - [25] Y. Li and C. Bruder, *Physical Review A* **77**, 015403 (2008).
 - [26] N. V. Vitanov and M. Drewsen, *Physical review letters* **122**, 173202 (2019).
 - [27] Y.-H. Kang, Z.-C. Shi, J. Song, and Y. Xia, *Optics Letters* **45**, 4952 (2020).
 - [28] J.-L. Wu, Y. Wang, J.-X. Han, C. Wang, S.-L. Su, Y. Xia, Y. Jiang, and J. Song, *Physical Review Applied* **13**, 044021 (2020).
 - [29] I. Tutunnikov, L. Xu, R. W. Field, K. A. Nelson, Y. Prior, and I. S. Averbukh, *Physical Review Research* **3**, 013249 (2021).
 - [30] W. Gerlach and O. Stern, *Zeitschrift für Physik* **9**, 349 (1922).
 - [31] J. Hirsch, *Physical review letters* **83**, 1834 (1999).
 - [32] Y. Li, C. Bruder, and C. Sun, *Physical review let-*

- ters **99**, 130403 (2007).
- [33] X. Li and M. Shapiro, The Journal of chemical physics **132**, 194315 (2010).
- [34] Y.-Y. Chen, C. Ye, Q. Zhang, and Y. Li, The Journal of Chemical Physics **152**, 204305 (2020).
- [35] C. L. Kane and E. J. Mele, Physical review letters **95**, 226801 (2005).
- [36] D. J. Thouless, M. Kohmoto, M. P. Nightingale, and M. den Nijs, Physical review letters **49**, 405 (1982).
- [37] M. Z. Hasan and C. L. Kane, Reviews of modern physics **82**, 3045 (2010).
- [38] M. H. Kolodrubetz, F. Nathan, S. Gazit, T. Morimoto, and J. E. Moore, Physical review letters **120**, 150601 (2018).
- [39] I. Mondragon-Shem, I. Martin, A. Alexandradinata, and M. Cheng, arXiv preprint arXiv:1811.10632 (2018).
- [40] F. Nathan, I. Martin, and G. Refael, Physical Review B **99**, 094311 (2019).
- [41] T. Oka and S. Kitamura, Annual Review of Condensed Matter Physics **10**, 387 (2019).
- [42] I. Martin, G. Refael, and B. Halperin, Physical Review X **7**, 041008 (2017).
- [43] M. Leibscher, T. F. Giesen, and C. P. Koch, The Journal of chemical physics **151**, 014302 (2019).
- [44] E. Boyers, P. J. Crowley, A. Chandran, and A. O. Sushkov, Physical Review Letters **125**, 160505 (2020).
- [45] See Supplemental Material, which includes Refs. [46,47], for (I) derivation of the first order correction terms to the adiabatic eigenstates and power spectrum, (II) derivation of the analytical expression for the enantioselective Chern number, (III) description of the Monte Carlo integration method used to calculate the orientationally averaged Chern number, and (IV) discussion of the laser shot noise limit for enantio TFC.
- [46] N. Goldman, E. Anisimovas, F. Gerbier, P. Öhberg, I. Spielman, and G. Juzeliūnas, New journal of physics **15**, 013025 (2013).
- [47] T. Andrijauskas, E. Anisimovas, M. Račiūnas, A. Mekys, V. Kudriašov, I. Spielman, and G. Juzeliūnas, Physical Review A **92**, 033617 (2015).
- [48] A. M. Samoilenko, *Elements of the mathematical theory of multi-frequency oscillations*, Vol. 71 (Springer Science & Business Media, 2012).
- [49] B. A. Bernevig and S.-C. Zhang, Physical review letters **96**, 106802 (2006).
- [50] J. A. Schellman, Chemical Reviews **75**, 323 (1975).
- [51] G. B. Park and R. W. Field, The Journal of chemical physics **144**, 200901 (2016).
- [52] F. Faure and B. Zhilinskii, Physical review letters **85**, 960 (2000).
- [53] K. Schwennicke and J. Yuen-Zhou, The Journal of Physical Chemistry C **124**, 4206 (2020).

Enantioselective Topological Frequency Conversion

Kai Schwennicke and Joel Yuen-Zhou

*Department of Chemistry and Biochemistry, University of California,
San Diego, La Jolla, California 92093, United States*

S1. ADIABATIC PERTURBATION THEORY

For completeness, we briefly review adiabatic perturbation theory. Let $|\tilde{\psi}(t)\rangle = \sum_l \tilde{c}_l(t)|\epsilon_l(t)\rangle$ be the solution of the time-dependent Schrödinger equation (TDSE) $i\hbar\partial_t|\tilde{\psi}(t)\rangle = \mathcal{H}(t)|\tilde{\psi}(t)\rangle$, where $\{|\epsilon_l(t)\rangle\}$ are the adiabatic eigenstates satisfying $\mathcal{H}(t)|\epsilon_l(t)\rangle = \epsilon_l(t)|\epsilon_l(t)\rangle$. Employing the TDSE, the following differential equation is obtained for $\tilde{c}_l(t)$,

$$i\hbar\dot{\tilde{c}}_l(t) = \epsilon_l(t)\tilde{c}_l(t) - i\hbar\sum_{l'}\langle\epsilon_l(t)|\boldsymbol{\omega}\cdot\nabla_{\boldsymbol{\omega}t}|\epsilon_{l'}(t)\rangle\tilde{c}_{l'}(t), \quad (\text{S1})$$

where $\boldsymbol{\omega} = (\omega_1, \omega_2)$. Ignoring non-adiabatic terms in Eq. S1 for $l' \neq l$,

$$\tilde{c}_l(t) \approx \tilde{c}_l(0)e^{-i\int_0^t dt' [\epsilon_l(t') - i\hbar\langle\epsilon_l(t')|\boldsymbol{\omega}\cdot\nabla_{\boldsymbol{\omega}t}|\epsilon_l(t')\rangle]/\hbar}. \quad (\text{S2})$$

Hereafter, we assume that the system is initialized in the l -th adiabatic state $|\tilde{\psi}(0)\rangle = |\epsilon_l(0)\rangle$. Eq. S2 is a statement of the adiabatic theorem and implies that the system shall remain in the l -th adiabatic state, $|\tilde{\psi}(t)\rangle \approx (\text{phase factor}) \times |\epsilon_l(t)\rangle$.

However, we are interested in $O(\hbar\omega)$ non-adiabatic corrections to Eq. S2. We rewrite $\tilde{c}_{l'} = \hbar\omega\tilde{c}_{l'}(t)a_{l'}(t)$ for $l' \neq l$,

$$|\tilde{\psi}(t)\rangle = \tilde{c}_l(t)[|\epsilon_l(t)\rangle + \sum_{l' \neq l} \hbar\omega a_{l'}(t)|\epsilon_{l'}(t)\rangle], \quad (\text{S3})$$

and insert this ansatz into Eq. S1,

$$\epsilon_l(t)\tilde{c}_l(t)a_{l'}(t)\hbar\omega + O(\hbar^2\omega^2) = \hbar\omega\epsilon_{l'}(t)\tilde{c}_l(t)a_{l'}(t) - i\hbar\langle\epsilon_{l'}(t)|\boldsymbol{\omega}\cdot\nabla_{\boldsymbol{\omega}t}|\epsilon_l(t)\rangle\tilde{c}_l(t) + O(\hbar^2\omega^2), \quad (\text{S4})$$

where we used $\dot{a}_{l'}(t) = \hbar\boldsymbol{\omega}\cdot\nabla_{\boldsymbol{\omega}t}a_{l'}(t)$. Solving for $a_{l'}(t)$, the $O(\hbar\omega)$ wavefunction is,

$$|\tilde{\psi}(t)\rangle = \tilde{c}_l(t) \left[|\epsilon_l(t)\rangle - i\hbar\sum_{l' \neq l} \frac{|\epsilon_{l'}(t)\rangle\langle\epsilon_{l'}(t)|\boldsymbol{\omega}\cdot\nabla_{\boldsymbol{\omega}t}|\epsilon_l(t)\rangle}{\epsilon_l(t) - \epsilon_{l'}(t)} \right]. \quad (\text{S5})$$

Calculating $\mathcal{P}_{av}(\omega_1)$ and $\mathcal{P}_{av}(\omega_2)$

Here, $\langle\tilde{\psi}(t)|\partial_{\omega_i t}\mathcal{H}(t)|\tilde{\psi}(t)\rangle$ and $P_{av}(\omega_i)$ are derived when the system is initiated in the adiabatic state $|\epsilon_l(0)\rangle$ and evolved near the adiabatic limit. Employing Eq. S5 for $|\tilde{\psi}(t)\rangle$, and making the change of variables $(\omega_1 t, \omega_2 t) = (\theta_1, \theta_2)$, the following expression to $O(\hbar\omega)$ is obtained:

$$\begin{aligned} \langle\tilde{\psi}(t)|\nabla_{\boldsymbol{\omega}t}\mathcal{H}(t)|\tilde{\psi}(t)\rangle &= \langle\epsilon_l(\boldsymbol{\theta})|\nabla_{\boldsymbol{\theta}}\mathcal{H}(\boldsymbol{\theta})|\epsilon_l(\boldsymbol{\theta})\rangle - \left\{ i\hbar\sum_{l' \neq l} \frac{\langle\epsilon_l(\boldsymbol{\theta})|\nabla_{\boldsymbol{\theta}}\mathcal{H}(\boldsymbol{\theta})|\epsilon_{l'}(t)\rangle\langle\epsilon_{l'}(\boldsymbol{\theta})|\boldsymbol{\omega}\cdot\nabla_{\boldsymbol{\theta}}|\epsilon_l(\boldsymbol{\theta})\rangle}{\epsilon_l(\boldsymbol{\theta}) - \epsilon_{l'}(\boldsymbol{\theta})} + \text{h.c.} \right\} \\ &= \nabla_{\boldsymbol{\theta}}\epsilon_l(\boldsymbol{\theta}) - \left\{ i\hbar\langle\nabla_{\boldsymbol{\theta}}\epsilon_l(\boldsymbol{\theta})|\boldsymbol{\omega}\cdot\nabla_{\boldsymbol{\theta}}|\epsilon_l(\boldsymbol{\theta})\rangle + \text{h.c.} \right\} \\ &= \nabla_{\boldsymbol{\theta}}\epsilon_l(\boldsymbol{\theta}) - \hbar\boldsymbol{\omega} \times \hat{\boldsymbol{v}}_{\perp}\Omega_l(\boldsymbol{\theta}), \end{aligned} \quad (\text{S6})$$

where $\boldsymbol{\omega} \times \hat{\boldsymbol{v}}_{\perp} = (\omega_2, -\omega_1)$ and $\Omega_l(\boldsymbol{\theta}) = i\langle\partial_{\theta_1}\epsilon_l(\boldsymbol{\theta})|\partial_{\theta_2}\epsilon_l(\boldsymbol{\theta})\rangle + \text{h.c.}$ is the Berry curvature of the l -th band.

S2. ANALYTICAL EVALUATION OF CHERN NUMBERS

Here, we analytically compute the Chern numbers for the bands of the system in the main text when

$\delta = 0$. We follow the procedure described in [S1]. We first consider the three-level Hamiltonian:

$$\mathcal{H}(\boldsymbol{\theta}) = \sum_{s=\pm 1} sh_3(\boldsymbol{\theta})|s\rangle\langle s| + \left\{ [h_1(\boldsymbol{\theta}) - ish_2(\boldsymbol{\theta})]|s\rangle\langle 0| + \text{h.c.} \right\}, \quad (\text{S7})$$

where $h_1(\boldsymbol{\theta})$, $h_2(\boldsymbol{\theta})$, $h_3(\boldsymbol{\theta})$ are real valued. Next, we invoke the unitary transformation $U(\boldsymbol{\theta}) = \sum_{s=0,\pm 1} e^{is\alpha(\boldsymbol{\theta})}|s\rangle\langle s|$, such that $\tan \alpha(\boldsymbol{\theta}) = h_2(\boldsymbol{\theta})/h_1(\boldsymbol{\theta})$, to define the real valued Hamiltonian,

$$\begin{aligned} \mathcal{H}'(\boldsymbol{\theta}) &= U(\boldsymbol{\theta})\mathcal{H}(\boldsymbol{\theta})U^\dagger(\boldsymbol{\theta}) \\ &= \sum_{s=\pm 1} sh_3(\boldsymbol{\theta})|s\rangle\langle s| + \sqrt{h_1^2(\boldsymbol{\theta}) + h_2^2(\boldsymbol{\theta})}(|s\rangle\langle 0| + \text{h.c.}). \end{aligned} \quad (\text{S8})$$

A set of eigenstates for $\mathcal{H}'(\boldsymbol{\theta})$ can be defined as $|\epsilon'_l(\boldsymbol{\theta})\rangle = \sum_{s=0,\pm 1} c_{l,s}(\boldsymbol{\theta})|s\rangle$, where the coefficients $c_{l,s}(\boldsymbol{\theta})$ are real. The eigenstates of $\mathcal{H}(\boldsymbol{\theta})$ are

$$|\epsilon_l(\boldsymbol{\theta})\rangle = U^\dagger(\boldsymbol{\theta})|\epsilon'_l(\boldsymbol{\theta})\rangle = \sum_{s=0,\pm 1} c_{l,s}(\boldsymbol{\theta})e^{-is\alpha(\boldsymbol{\theta})}|s\rangle. \quad (\text{S9})$$

The Berry connection for the l -th band is

$$\begin{aligned} \mathbf{A}_l(\boldsymbol{\theta}) &= i\langle \epsilon_l(\boldsymbol{\theta}) | \nabla_{\boldsymbol{\theta}} | \epsilon_l(\boldsymbol{\theta}) \rangle \\ &= \nabla_{\boldsymbol{\theta}} \alpha(\boldsymbol{\theta}) \sum_{s=\pm 1} sc_{l,s}^2(\boldsymbol{\theta}), \end{aligned} \quad (\text{S10})$$

where we used the fact that $\sum_{s=0,\pm 1} c_{l,s}(\boldsymbol{\theta}) \nabla_{\boldsymbol{\theta}} c_{l,s}(\boldsymbol{\theta}) = \frac{1}{2} \nabla_{\boldsymbol{\theta}} \sum_{s=0,\pm 1} |c_{l,s}|^2 = 0$. The Berry curvature is defined as the z -component of the curl of the Berry connection, *i.e.*, $\Omega_l(\boldsymbol{\theta}) = (\nabla_{\boldsymbol{\theta}} \times \mathbf{A}_l(\boldsymbol{\theta})) \cdot \hat{z}$. Note that there are singularities in the Berry connection when $\nabla_{\boldsymbol{\theta}} \alpha(\boldsymbol{\theta}) = \frac{h_1(\boldsymbol{\theta}) \nabla_{\boldsymbol{\theta}} h_2(\boldsymbol{\theta}) - h_2(\boldsymbol{\theta}) \nabla_{\boldsymbol{\theta}} h_1(\boldsymbol{\theta})}{h_1^2(\boldsymbol{\theta}) + h_2^2(\boldsymbol{\theta})}$ is undefined; they occur at the critical points where $h_1(\boldsymbol{\theta}) = h_2(\boldsymbol{\theta}) = 0$.

Considering Eqs. 5 and 6 from the main text and taking $\delta = 0$, the values $h_1(\boldsymbol{\theta})$, $h_2(\boldsymbol{\theta})$, $h_3(\boldsymbol{\theta})$ are

$$\begin{aligned} h_1(\boldsymbol{\theta}) &= -\frac{\boldsymbol{\mu}_{21} \cdot \mathbf{E}_{21} \sin(\theta_1)}{2\sqrt{2}}, \\ h_2(\boldsymbol{\theta}) &= -\frac{\boldsymbol{\mu}_{32} \cdot \mathbf{E}_{32} \sin(\theta_2)}{2\sqrt{2}}, \\ h_3(\boldsymbol{\theta}) &= -\frac{1}{2} \boldsymbol{\mu}_{31} \cdot \mathbf{E}_{31} [m - \cos(\theta_1) - \cos(\theta_2)], \end{aligned} \quad (\text{S11})$$

and the aforementioned singularities occur at the $\boldsymbol{\theta} = (\theta_1, \theta_2)$ values $\boldsymbol{\theta}_{00} = (0, 0)$, $\boldsymbol{\theta}_{0\pi} = (0, \pi)$, $\boldsymbol{\theta}_{\pi 0} = (\pi, 0)$, and $\boldsymbol{\theta}_{\pi\pi} = (\pi, \pi)$. Physically, these critical points indicate geometric conditions where certain components of light-matter coupling vanish.

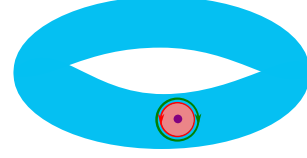


Figure S1: *Contour integration procedure to evaluate Chern number C_l .* The closed curve ∂_R bounds both the pink region, which contains the singularity of $\mathbf{A}_l(\boldsymbol{\theta})$, and the blue region, which is rest of the torus. To apply Stokes theorem, we integrate counter-clockwise (red curve) along ∂_R to find the surface integral for the pink region, and clockwise along ∂_R (green curve) to find the surface integral for the blue region. The procedure can be extended to an arbitrary number of singularities of $\mathbf{A}_l(\boldsymbol{\theta})$.

The Chern number is proportional to the surface integral of the Berry curvature over the torus \mathbb{T} ,

$$C_l = \frac{1}{2\pi} \int_{\mathbb{T}} d\boldsymbol{\theta} \Omega_l(\boldsymbol{\theta}). \quad (\text{S12})$$

Using Stokes theorem, it can be written as a contour integral of the Berry connection; however, the singularities must be removed. To motivate the general procedure, first consider the case where the Berry connection $\mathbf{A}_l(\boldsymbol{\theta})$ contains only one singularity. The curve ∂_R can be drawn, such that it defines an infinitesimal region containing the singularity (region I) and the rest of the torus (region II) (see Fig. S1). Applying a gauge transformation $|\epsilon_l(\boldsymbol{\theta})\rangle \rightarrow e^{i\phi_l(\boldsymbol{\theta})} |\epsilon_l(\boldsymbol{\theta})\rangle$ in region I can remove the singularity, $A_l(\boldsymbol{\theta}) \rightarrow \mathbf{A}'_l(\boldsymbol{\theta}) = \mathbf{A}_l(\boldsymbol{\theta}) - \nabla_{\boldsymbol{\theta}} \phi_l(\boldsymbol{\theta})$, while the Berry curvature is unaffected [S1, S2]. Taking $\nabla_{\boldsymbol{\theta}} \phi_l(\boldsymbol{\theta}) = \mathbf{A}_l(\boldsymbol{\theta})$ achieves this desired result. The Chern numbers can then be written as the

summation of contour integrals for each region:

$$\begin{aligned}
C_l &= \frac{1}{2\pi} \int_{\mathbb{T}} d\boldsymbol{\theta} \Omega_l(\boldsymbol{\theta}) \\
&= \frac{1}{2\pi} \oint_{\partial_R} d\boldsymbol{\theta} \cdot \mathbf{A}'_l(\boldsymbol{\theta}) - \frac{1}{2\pi} \oint_{\partial_R} d\boldsymbol{\theta} \cdot \mathbf{A}_l(\boldsymbol{\theta}) \\
&= \frac{1}{2\pi} \oint_{\partial_R} d\boldsymbol{\theta} \cdot [\mathbf{A}_l(\boldsymbol{\theta}) - \nabla_{\boldsymbol{\theta}} \phi_l(\boldsymbol{\theta})] - \frac{1}{2\pi} \oint_{\partial_R} d\boldsymbol{\theta} \cdot \mathbf{A}_l(\boldsymbol{\theta}) \\
&= -\frac{1}{2\pi} \oint_{\partial_R} d\boldsymbol{\theta} \cdot \nabla_{\boldsymbol{\theta}} \phi_l(\boldsymbol{\theta}) \\
&= -\frac{1}{2\pi} \oint_{\partial_R} d\boldsymbol{\theta} \cdot \mathbf{A}_l(\boldsymbol{\theta}). \tag{S13}
\end{aligned}$$

In going from the first to the second line, we applied Stokes theorem in region I by traversing ∂_R in a counterclockwise fashion, and in region II by doing so in a clockwise way (see Fig. S1).

If the Berry connection \mathbf{A}_l contains multiple singularities $\boldsymbol{\theta}_{ij}$, then local gauge transformations must be carried out in multiple regions to remove all of them. Then the Chern number results in

$$C_l = - \sum_{ij} \frac{1}{2\pi} \oint_{\partial_{R_{ij}}} d\boldsymbol{\theta} \cdot \mathbf{A}_l(\boldsymbol{\theta}) \tag{S14}$$

where the curves $\{\partial_{R_{ij}}\}$ enclose an infinitesimal region around each of the singularities $\boldsymbol{\theta}_{ij}$. Therefore, the Chern number can be calculated by studying the behavior of $\mathbf{A}_l(\boldsymbol{\theta})$ near the singularities.

Let $\mathbf{q} = (q_1, q_2)$ be a small displacement from the point $\boldsymbol{\theta}_{ij}$. Since $\sin(x) \approx x$ and $\sin(\pi + x) \approx -x$ as $x \rightarrow 0$, then

$$\begin{aligned}
\alpha(\boldsymbol{\theta}_{00} + \mathbf{q}) &\approx \beta, \\
\alpha(\boldsymbol{\theta}_{0\pi} + \mathbf{q}) &\approx -\beta, \\
\alpha(\boldsymbol{\theta}_{\pi 0} + \mathbf{q}) &\approx -\beta, \\
\alpha(\boldsymbol{\theta}_{\pi\pi} + \mathbf{q}) &\approx \beta, \tag{S15}
\end{aligned}$$

where $\tan \beta = \frac{\boldsymbol{\mu}_{32} \cdot \mathbf{E}_{32} q_2}{\boldsymbol{\mu}_{21} \cdot \mathbf{E}_{21} q_1}$. The gradients $\nabla_{\mathbf{q}} \alpha(\boldsymbol{\theta})$ near the critical points can be readily evaluated in polar

coordinates, $|\mathbf{q}|e^{i\gamma} = q_1 + iq_2$,

$$\begin{aligned}
\nabla_{\mathbf{q}} \alpha(\boldsymbol{\theta}_{00} + \mathbf{q}) &= -\nabla_{\mathbf{q}} \alpha(\boldsymbol{\theta}_{\pi 0} + \mathbf{q}) \\
&= -\nabla_{\mathbf{q}} \alpha(\boldsymbol{\theta}_{0\pi} + \mathbf{q}) \\
&= \nabla_{\mathbf{q}} \alpha(\boldsymbol{\theta}_{\pi\pi} + \mathbf{q}) \\
&\approx \frac{1}{|\mathbf{q}|} \frac{(\boldsymbol{\mu}_{21} \cdot \mathbf{E}_{21})(\boldsymbol{\mu}_{32} \cdot \mathbf{E}_{32})}{(\boldsymbol{\mu}_{21} \cdot \mathbf{E}_{21})^2 \cos^2 \gamma + (\boldsymbol{\mu}_{32} \cdot \mathbf{E}_{32})^2 \sin^2 \gamma} \hat{\gamma}. \tag{S16}
\end{aligned}$$

The line integral of $\nabla_{\mathbf{q}} \alpha(\boldsymbol{\theta}_{00} + \mathbf{q})$ over a small circle in the limit when $|\mathbf{q}| \rightarrow 0$,

$$\begin{aligned}
&\oint_{|\mathbf{q}| \rightarrow 0} d\mathbf{q} \cdot \nabla_{\mathbf{q}} \alpha(\boldsymbol{\theta}_{00} + \mathbf{q}) \\
&= \left(\int_0^{\pi/2^-} d\gamma + \int_{\pi/2^+}^{3\pi/2^-} d\gamma \right. \\
&\quad \left. + \int_{3\pi/2^+}^{2\pi} d\gamma \right) \frac{(\boldsymbol{\mu}_{21} \cdot \mathbf{E}_{21})(\boldsymbol{\mu}_{32} \cdot \mathbf{E}_{32})}{(\boldsymbol{\mu}_{21} \cdot \mathbf{E}_{21})^2 \cos^2 \gamma + (\boldsymbol{\mu}_{32} \cdot \mathbf{E}_{32})^2 \sin^2 \gamma} \\
&= \left(\int_0^{\text{sgn}[(\boldsymbol{\mu}_{21} \cdot \mathbf{E}_{21})(\boldsymbol{\mu}_{32} \cdot \mathbf{E}_{32})]^\infty} dx + \int_{-\text{sgn}[(\boldsymbol{\mu}_{21} \cdot \mathbf{E}_{21})(\boldsymbol{\mu}_{32} \cdot \mathbf{E}_{32})]^\infty}^{\text{sgn}[(\boldsymbol{\mu}_{21} \cdot \mathbf{E}_{21})(\boldsymbol{\mu}_{32} \cdot \mathbf{E}_{32})]^\infty} dx \right. \\
&\quad \left. + \int_{-\text{sgn}[(\boldsymbol{\mu}_{21} \cdot \mathbf{E}_{21})(\boldsymbol{\mu}_{32} \cdot \mathbf{E}_{32})]^\infty}^0 dx \right) \frac{1}{1+x^2} \\
&= 2\pi \text{sgn}[(\boldsymbol{\mu}_{21} \cdot \mathbf{E}_{21})(\boldsymbol{\mu}_{32} \cdot \mathbf{E}_{32})]. \tag{S17}
\end{aligned}$$

In the second line, we split the integral into three parts, noticing that the integral in the remaining infinitesimal regions around $\gamma = \pi/2$ and $\gamma = 3\pi/2$ vanish given that the integrand is finite, $\int_{\pi/2^-}^{\pi/2^+} d\gamma(\cdot) = \int_{3\pi/2^-}^{3\pi/2^+} d\gamma(\cdot) = 0$. In the third line, we let $x = \frac{\boldsymbol{\mu}_{32} \cdot \mathbf{E}_{32}}{\boldsymbol{\mu}_{21} \cdot \mathbf{E}_{21}} \tan \gamma$, and $dx = \frac{\boldsymbol{\mu}_{32} \cdot \mathbf{E}_{32}}{\boldsymbol{\mu}_{21} \cdot \mathbf{E}_{21}} \sec^2 \gamma d\gamma$ and recognized that $x \rightarrow \text{sgn}[(\boldsymbol{\mu}_{21} \cdot \mathbf{E}_{21})(\boldsymbol{\mu}_{32} \cdot \mathbf{E}_{32})]^\infty$ as $\gamma \rightarrow (\pi/2)^-, (3\pi/2)^-$ and $x \rightarrow -\text{sgn}[(\boldsymbol{\mu}_{21} \cdot \mathbf{E}_{21})(\boldsymbol{\mu}_{32} \cdot \mathbf{E}_{32})]^\infty$ as $\gamma \rightarrow (\pi/2)^+, (3\pi/2)^+$.

The procedure of Eqs. (S16) and (S17) can be repeated for the other critical points, yielding,

$$\begin{aligned}
\oint_{|\mathbf{q}| \rightarrow 0} d\mathbf{q} \nabla_{\mathbf{q}} \alpha(\boldsymbol{\theta}_{0\pi} + \mathbf{q}) &= -2\pi \text{sgn}[(\boldsymbol{\mu}_{21} \cdot \mathbf{E}_{21})(\boldsymbol{\mu}_{32} \cdot \mathbf{E}_{32})], \\
\oint_{|\mathbf{q}| \rightarrow 0} d\mathbf{q} \nabla_{\mathbf{q}} \alpha(\boldsymbol{\theta}_{\pi 0} + \mathbf{q}) &= -2\pi \text{sgn}[(\boldsymbol{\mu}_{21} \cdot \mathbf{E}_{21})(\boldsymbol{\mu}_{32} \cdot \mathbf{E}_{32})], \\
\oint_{|\mathbf{q}| \rightarrow 0} d\mathbf{q} \nabla_{\mathbf{q}} \alpha(\boldsymbol{\theta}_{\pi\pi} + \mathbf{q}) &= 2\pi \text{sgn}[(\boldsymbol{\mu}_{21} \cdot \mathbf{E}_{21})(\boldsymbol{\mu}_{32} \cdot \mathbf{E}_{32})]. \tag{S18}
\end{aligned}$$

Using Eqs. S10 and S14, the Chern number for the l -th band is

$$C_l = -\text{sgn}[(\boldsymbol{\mu}_{21} \cdot \mathbf{E}_{21})(\boldsymbol{\mu}_{32} \cdot \mathbf{E}_{32})] \sum_{s=\pm 1} s [c_{l,s}^2(\boldsymbol{\theta}_{00}) - c_{l,s}^2(\boldsymbol{\theta}_{0\pi}) - c_{l,s}^2(\boldsymbol{\theta}_{\pi 0}) + c_{l,s}^2(\boldsymbol{\theta}_{\pi\pi})] \quad (\text{S19})$$

For $|m| < 2$ the Chern numbers for the upper, middle, and lower adiabatic states can be seen to yield,

$$\begin{aligned} C_U &= -2\text{sgn}[m(\boldsymbol{\mu}_{21} \cdot \mathbf{E}_{21})(\boldsymbol{\mu}_{32} \cdot \mathbf{E}_{32})(\boldsymbol{\mu}_{31} \cdot \mathbf{E}_{31})], \\ C_M &= 0, \\ C_L &= 2\text{sgn}[m(\boldsymbol{\mu}_{21} \cdot \mathbf{E}_{21})(\boldsymbol{\mu}_{32} \cdot \mathbf{E}_{32})(\boldsymbol{\mu}_{31} \cdot \mathbf{E}_{31})]. \end{aligned} \quad (\text{S20})$$

For $|m| > 2$, all $C_l = 0$.

S3. ISOTROPIC AVERAGING OF CHERN NUMBERS

Here, we describe the Monte Carlo integration method used to compute the distribution of lower band Chern numbers for the R -enantiomer. As stated in the main text, the orientationally averaged Chern number is computed as

$$\langle C_L^R \rangle = \frac{1}{8\pi^2} \int_0^{2\pi} \int_0^{2\pi} \int_0^\pi d\chi d\phi d\theta C_L^R(\chi, \phi, \theta) \sin(\theta), \quad (\text{S21})$$

where the molecule orientation with respect to the driving electric field is specified by the Euler angles χ, ϕ, θ . Consider the average of a function $f(x, y, z)$ over the intervals $x \in [a, b]$, $y \in [c, d]$, $z \in [l, m]$:

$$f_{av} = \frac{1}{V} \int_a^b \int_c^d \int_l^m dx dy dz f(x, y, z), \quad (\text{S22})$$

where $V = (b - a)(d - c)(m - l)$ is the volume over which the function is integrated. f_{av} can be approximated by randomly sampling a large enough set of N points within V and calculating the average of the value of $f(x, y, z)$:

$$f_{av} \approx \frac{1}{N} \sum_{i=1}^N f(x_i, y_i, z_i). \quad (\text{S23})$$

Thus,

$$\int_a^b \int_c^d \int_l^m dx dy dz f(x, y, z) = \lim_{N \rightarrow \infty} \frac{V}{N} \sum_{i=1}^N f(x_i, y_i, z_i) \quad (\text{S24})$$

For our calculations, we set $f(\chi, \phi, \theta) = C_l^R(\chi, \phi, \theta) \sin \theta$. Using the prescription of Eq.

S24, Eq. S21 can be approximated as

$$\langle C_L^R \rangle \approx \frac{1}{8\pi^2} \frac{V}{N} \sum_{i=1}^N C_L^R(\chi_i, \phi_i, \theta_i) \sin \theta_i$$

where $V = 4\pi^3$. For the calculations in the main text, each Monte Carlo simulation consisted of $N = 10^4$ randomly selected orientations from a uniform distribution of χ, ϕ, θ values. In total, 1188 individual simulations were carried out, from which an average and standard deviation for $\langle C_L^R \rangle$ were extracted (see Fig. S2). Employing a z-test with a 95% confidence interval, the expectation value was found to be $\langle C_L^R \rangle = 1.311 \pm 0.001$. When $\delta = 0$, the result we obtain is $\langle C_L^R \rangle = 1.333 \pm 0.001$, which we conjecture to be $\frac{4}{3}$.

S4. LASER SHOT-NOISE

The laser shot noise is defined as the width of the photon distribution of the driving field. In the main text the laser field strength is assumed to be approximately $E = 10^{-9}$ a.u., or $500 \frac{\text{V}}{\text{m}}$. Assuming that the laser-beam waist area is $A = 1 \text{cm}^2$, its power is given by,

$$\begin{aligned} P &= \frac{cA\epsilon_0 E^2}{8\pi} \\ &= \frac{3 \times 10^8 \frac{\text{m}}{\text{s}} \times 1 \text{cm}^2 \times \frac{1 \text{m}^2}{100^2 \text{cm}^2} \times 8.85 \times 10^{-12} \frac{\text{C}^2}{\text{J}\cdot\text{m}} \times (500 \frac{\text{V}}{\text{m}})^2}{8\pi} \\ &= 3 \text{mW} \end{aligned} \quad (\text{S25})$$

where c is the speed of light and ϵ_0 is the permittivity of free space. The frequencies of the molecular transitions in the main text are on the order of $\nu = 10$ GHz. Then the expected number of photons produced by the laser after a long enough time $t^* = 2000 \times 2\pi/\omega_2$ which guarantees TFC is

$$N = \frac{Pt^*}{h\nu} = \frac{3 \times 10^{-3} \text{W} \times 8 \times 10^{-3} \text{s}}{6.36 \times 10^{-34} \text{J}\cdot\text{s} \times 10 \times 10^9 \text{s}^{-1}} = 4 \times 10^{18} \quad (\text{S26})$$

The photon distribution is taken to be Poissonian. The standard deviation of this distribution is \sqrt{N} , so the laser shot noise is $\sqrt{N} \sim 10^9$.

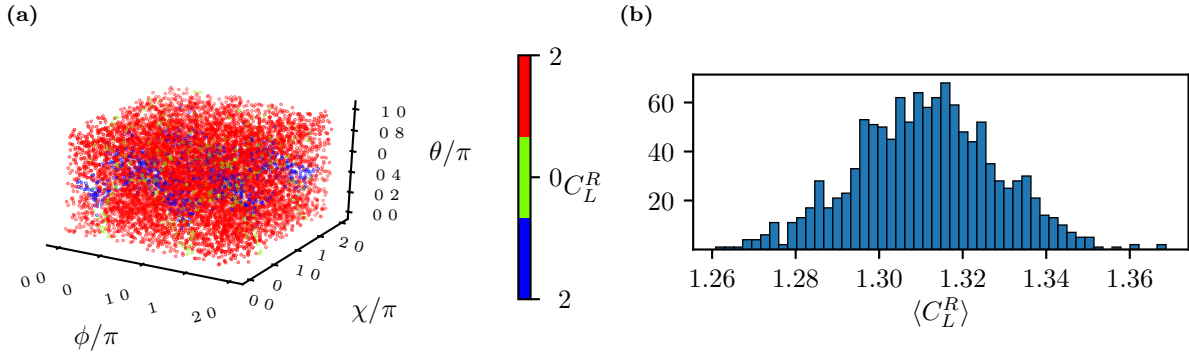


Figure S2: *Isotropic averaging of Chern numbers.* (a) A Monte Carlo simulation consists of choosing 10^4 random orientations (specified by θ, ϕ, χ) and evaluating C_L^R for each of them. Each simulation outputs an average Chern number $\langle C_L^R \rangle$. (b) Distribution of $\langle C_L^R \rangle$ across 1188 simulations.

[S1] T. Andrijauskas, E. Anisimovas, M. Račiūnas, A. Mekys, V. Kudriašov, I. Spielman, and G. Juzeliūnas, *Physical Review A* **92**, 033617 (2015).

[S2] N. Goldman, E. Anisimovas, F. Gerbier, P. Öhberg, I. Spielman, and G. Juzeliūnas, *New journal of physics* **15**, 013025 (2013).